

Reducing Textural Bias Improves Robustness of Deep Segmentation CNNs

Seoin Chai, Daniel Rueckert, and Ahmed E. Fetit

Imperial College London, London, United Kingdom

Abstract. Despite current advances in deep learning, domain shift remains a common problem in medical imaging settings. Recent findings on natural images suggest that deep neural models can show a textural bias when carrying out image classification tasks, which goes against the common understanding of convolutional neural networks (CNNs) recognising objects through increasingly complex representations of shape. This study draws inspiration from recent findings on natural images and aims to investigate ways in which addressing the textural bias phenomenon could be used to bring up the robustness and transferability of deep segmentation models when applied to three-dimensional (3D) medical data. To achieve this, publicly available MRI scans from the Developing Human Connectome Project are used to investigate ways in which simulating textural noise can help train robust models in a complex segmentation task. Our findings illustrate how applying specific types of textural filters prior to training the models can increase their ability to segment scans corrupted by previously unseen noise.

Keywords: Textural bias · Segmentation · Domain shift · Neuroimaging

1 Introduction

In medical imaging research settings, using convolutional neural networks (CNNs) is a popular way of classifying and segmenting radiological scans. However, radiological scans can contain subtle visual noise due to the way they are acquired, which can often obscure the performance of *texture-biased* CNNs. Another critical problem is that whilst a network may be optimised to perform well on images of one domain, performance often degrades when applied on images from a different domain [6], e.g. a different hospital or imaging centre; such problem arises for various reasons, including variations in acquisition protocols or scanner manufacturer hardware. In a study on natural images by Geirhos et al., separate CNNs were trained on standard ImageNet data as well as a stylised version of the same data, introducing conflicting textures to the input images. In doing so, the authors showed that training networks on stylised images has led to a reduction of the textural bias phenomenon [2]. In this study, we draw inspiration from the work reported in [2] and hypothesise that addressing the textural bias phenomenon can improve robustness of CNNs in medical settings.

With the ultimate goal of training a CNN that is robust to domain shift in medical settings, we carried out an empirical investigation using MRI scans

publicly available from the Developing Human Connectome Project (DHCP). In doing so, we simulated different categories and levels of textural noise by applying several permutations of filtering techniques to the scans. Eleven models were trained and subsequently tested on seventeen different held-out sets in order to evaluate which settings can best generalise to previously unseen noise, thereby thoroughly simulating performance under various degrees of domain shift.

2 Materials and Methods

2.1 Dataset

Seventy publicly available neonatal MRI scans from the DHCP cohort (<http://www.developingconnectome.org/project/>) [11] were used in this investigation. The data consisted of 3D T2-weighted scans and segmentation maps corresponding to ten classes, including the background. Nine classes represent brain tissues: cerebrospinal fluid, cortical grey matter, white matter, background bordering brain tissues, ventricles, cerebellum, deep grey matter, brainstem and hippocampus. The scans vary in shape and intensity because the brain rapidly changes during development and the scans represent 24.3-42.2 week old subjects. Fig. 1 shows an example T2-weighted scan and corresponding labels. All scans were normalised to zero-mean and unit-variance before they are used to train the models which will be called t2norm from now. Of the seventy scans provided, fifty were used for training, ten for validation, and ten for testing.

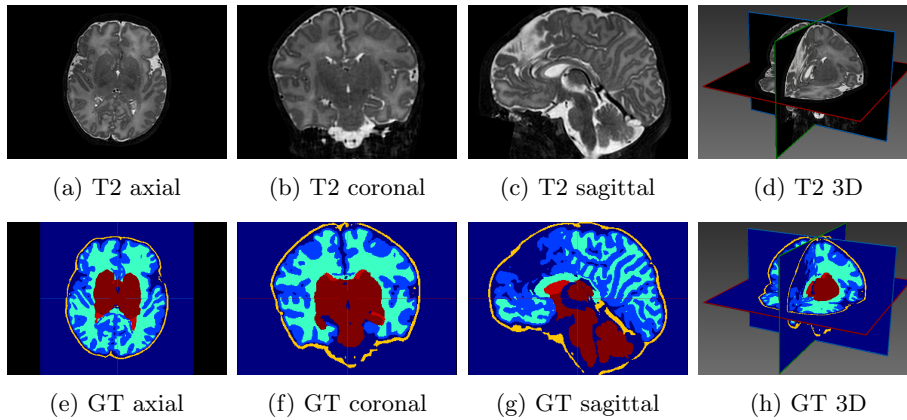


Fig. 1: Example T2-weighted neonatal brain scan and corresponding segmentation labels (GT) from the DHCP dataset.

2.2 Textural Noise Simulation

The first smoothing method used is Gaussian blur, which is produced by continuously applying a Gaussian filter to the image. The result resembles looking at an image behind a translucent screen hence the filter is often used to denoise images. Different degrees of blurring can be obtained by rendering the σ value from the Eq. (1) [13] where higher values of σ gives blurrier transformations. In the experiment, scikit-image library's [14] build-in function, `skimage.filters.gaussian()` was used. This was carried out five times each with σ values 1, 2, 3, 4 and 5 to give five different degrees of Gaussian blurred datasets (named gaus1, gaus2, gaus3, gaus4, and gaus5 respectively). Fig. 2 shows example noisy images.

$$f(x, y, z) = \left(\frac{1}{2\pi\sigma^2}\right)^{\frac{3}{2}} \exp\left(-\frac{x^2}{2\sigma^2} - \frac{y^2}{2\sigma^2} - \frac{z^2}{2\sigma^2}\right) \quad (1)$$

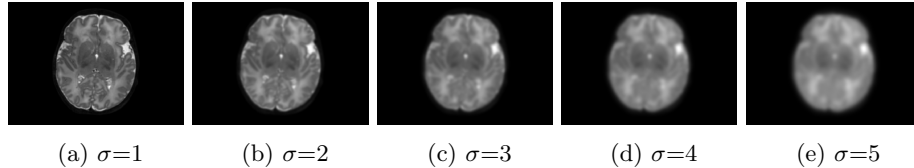


Fig. 2: Axial slices of Gaussian blurred brain images with $\sigma=1, 2, 3, 4$ and 5 .

Second, we used median filters, which replace the pixel value with the median of the neighbouring pixels. The function `scipy.ndimage.median_filter()` was used which takes in a variable called `size` which specifies the distance from the current pixel to the pixels that will be taken into account in generating median. Hence, higher values of `size` give smoother images. Three different degrees of median filtered images each with `size` values 2, 5 and 8 were generated (named median2, median5 and median8 respectively). Fig. 3 shows example noisy images.

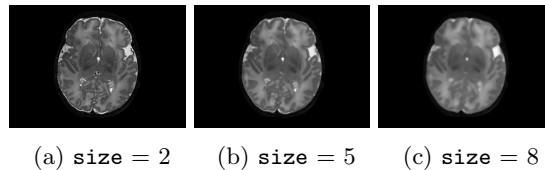


Fig. 3: Axial slices of median smoothed images with `size = 2, 5` and `8`.

The speckle generating filter used in the experiment is called Salt and Pepper (SNP) filter which randomly generates black and white pixels on the image. The function used was written in python and takes in a value called `prob` between

0 and 0.5. SNP method generates a random number for each pixel and if it is less than `prob` it paints the pixel with black, if it is greater than `1-prob` it paints the pixel with white, otherwise the pixel is left untouched. The higher the value of `prob` is, the noisier the image gets. Again, `t2norm` images were used with `prob` values 0.01, 0.03, 0.05, 0.07, 0.1, 0.15 and 0.2 to create seven different noisy datasets (named `snp01`, `snp03`, `snp05`, `snp07`, `snp10`, `snp15` and `snp20` respectively). Examples from those datasets can be found in Fig. 4.

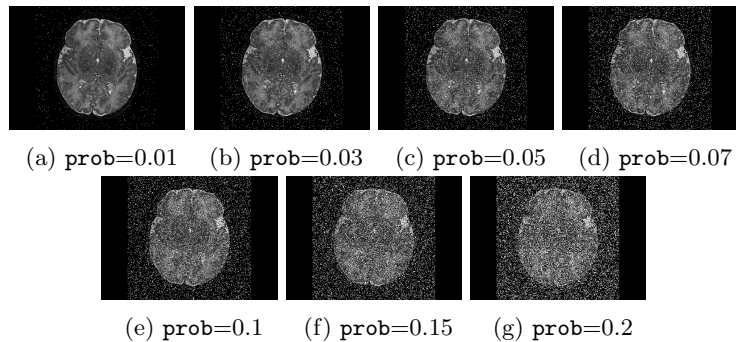


Fig. 4: Axial slices of Salt and Pepper applied images with `prob`=0.01, 0.03, 0.05, 0.07, 0.1, 0.15 and 0.2.

2.3 CNN Architecture

We used DeepMedic, an open source 3D architecture with multiple convolutional pathways built for brain lesion segmentation tasks [15]. The architecture we used in this investigation is inspired by the example in <https://github.com/deepmedic/deepmedic>. Eight layers are used in both the normal pathway and the subsampled pathways with the kernel size of 3^3 . Two parallel subsampled pathways are used, giving a total of three pathways. Residual connections are also used between layers 4 and 3, 6 and 5 and 8 and 7. The number of feature maps used in each FC layer was 250. The network ran for 100 epochs where each epoch comprised of 20 subepochs. In every subepoch, images from five cases were loaded and the training samples were extracted. Batch size used is 10, a predefined learning rate scheduler is used which schedules every eight epochs starting from the 24th epoch. Finally, RMSProp is used as the optimiser with L1 and L2 regularisation with values 10^{-5} and 10^{-4} .

2.4 Experiments

Since the motivation of the experiments is to find out whether training models in a certain textural noise setting could help with the domain shift problem,

some of the datasets created above were left untouched during model training. DeepMedic was hence trained on eleven different combinations of the following datasets: t2norm, gaus1, gaus3, gaus4, snp01, snp05, snp10 and median5 (Table 1). The unseen data reserved purely for testing are gaus2, gaus5, snp03, snp07, snp15, snp20, median2 and median8 (in sixteen different combinations).

Table 1: Model names and training dataset combinations.

Model Name	Data Combination
MODEL_T2Norm	t2norm
MODEL_GAUS1	gaus1
MODEL_GAUS3	gaus3
MODEL_GAUS4	gaus4
MODEL_GAUS134	gaus1, gaus3, gaus4
MODEL_SNP01	snp01
MODEL_SNP05	snp05
MODEL_SNP10	snp10
MODEL_SNP010510	snp01, snp05, snp10
MODEL_GAUS134_SNP010510	gaus1, gaus3, gaus4, snp01, snp05, snp10
MODEL_MEDIAN5	median5

3 Results and Discussion

All eleven models were first tested on held out data that represent the settings they were trained on. Models were then tested on held out data that represent settings that are completely new and are assumed to represent domain shift. For succinctness, three models showing the most insightful results are presented in tables in detail.

First, we observed that the model trained on the normal DHCP dataset achieved highest performance when segmenting the data it was trained on, and the data where the texture transformation was only lightly applied (Table 2). This suggests that the some of the images used for the experiment could be assumed to represent worst-case scenarios of domain shift. Models that were trained on images smoothed out by the Gaussian filter only seemed to generalise on Gaussian filtered images that were generated using similar values of σ as the images used for training, e.g. MODEL_GAUS3 only worked for gaus3 and gaus4, but not the other variations of the Gaussian images. When a model was trained on a Gaussian dataset created with a large value for σ , it did not even manage to segment the original DHCP data correctly. When a model was trained on multiple Gaussian datasets generated with a variety of σ values, it generalised well on the original DHCP as well as Gaussian filtered images, even for the cases where the σ value used were different from the ones used to create the training dataset; segmentation performance on the median filtered data also increased. However the model still did not quite reach an accurate

Table 2: MODEL_T2NORM DSC (not trained on textural noise) on the 16 held-out test datasets. The left-most column indicates which dataset was used for testing the model. Rows highlighted in green represent settings where the model achieves over 0.9 DSC for all classes.

Class	1	2	3	4	5	6	7	8	9	10
t2norm	0.9935	0.9599	0.9664	0.9757	0.9196	0.9539	0.9778	0.9706	0.9712	0.9298
gaus1	0.9887	0.9021	0.9197	0.9430	0.8643	0.9079	0.9597	0.9528	0.9567	0.8990
gaus2	0.9669	0.5418	0.3340	0.6559	0.7094	0.6257	0.5977	0.5665	0.8893	0.6608
gaus3	0.9498	0.1567	0.0384	0.5165	0.6083	0.2527	0.4442	0.4243	0.6900	0.1347
gaus4	0.9471	0.0078	0.0175	0.5341	0.5499	0.0025	0.3344	0.4549	0.1604	0.0000
gaus5	0.9398	0.0019	0.0161	0.4700	0.4544	0.0008	0.3581	0.3673	0.0033	0.0005
snp01	0.9922	0.8714	0.8502	0.8445	0.8962	0.8895	0.9402	0.8611	0.9251	0.8383
snp03	0.9396	0.4562	0.4808	0.1473	0.6321	0.1928	0.1685	0.0585	0.4776	0.1085
snp05	0.5533	0.2653	0.0663	0.0160	0.2390	0.0032	0.0001	0.0033	0.0179	0.0017
snp07	0.1699	0.2149	0.0003	0.0008	0.1238	0.0010	0.0000	0.0002	0.0001	0.0001
snp10	0.0303	0.0780	0.0000	0.0000	0.0405	0.0000	0.0000	0.0000	0.0000	0.0000
snp15	0.0015	0.0053	0.0000	0.0000	0.0024	0.0000	0.0000	0.0000	0.0000	0.0000
snp20	0.0002	0.0012	0.0000	0.0000	0.0001	0.0000	0.0000	0.0000	0.0000	0.0000
median2	0.9891	0.8754	0.8886	0.9258	0.8199	0.8895	0.9622	0.9522	0.9411	0.8833
median5	0.9918	0.8515	0.8657	0.9143	0.8850	0.8617	0.8959	0.9157	0.9481	0.8682
median8	0.9838	0.6175	0.4673	0.7358	0.7640	0.5942	0.5781	0.6340	0.8758	0.4814

Table 3: MODEL_SNP10 DSCs on the 16 test datasets. The left-most column indicates which dataset was used for testing the model. Rows highlighted in green represent settings where the model achieves over 0.9 DSC for all classes.

Class	1	2	3	4	5	6	7	8	9	10
t2norm	0.9930	0.9517	0.9584	0.9680	0.9115	0.9420	0.9725	0.9639	0.9638	0.9141
gaus1	0.9886	0.9037	0.9158	0.9374	0.8645	0.9080	0.9566	0.9466	0.9477	0.8877
gaus2	0.9732	0.5032	0.5560	0.6955	0.7164	0.7349	0.8767	0.8020	0.8931	0.8133
gaus3	0.9607	0.2073	0.1664	0.5998	0.5844	0.5244	0.8301	0.6976	0.8382	0.7118
gaus4	0.9555	0.0815	0.0777	0.5744	0.4809	0.2570	0.7799	0.6270	0.7166	0.5742
gaus5	0.9548	0.0340	0.0646	0.5626	0.3780	0.1207	0.7084	0.5604	0.4710	0.4167
snp01	0.9931	0.9534	0.9597	0.9694	0.9133	0.9461	0.9734	0.9654	0.9659	0.9173
snp03	0.9931	0.9559	0.9618	0.9713	0.9156	0.9498	0.9745	0.9674	0.9682	0.9226
snp05	0.9932	0.9575	0.9631	0.9727	0.9165	0.9511	0.9751	0.9681	0.9685	0.9250
snp07	0.9932	0.9583	0.9639	0.9736	0.9169	0.9500	0.9751	0.9684	0.9688	0.9271
snp10	0.9933	0.9586	0.9639	0.9739	0.9167	0.9514	0.9756	0.9684	0.9693	0.9272
snp15	0.9932	0.9551	0.9592	0.9711	0.9140	0.9451	0.9739	0.9666	0.9673	0.9208
snp20	0.9904	0.9408	0.9437	0.9609	0.8912	0.9357	0.9653	0.9559	0.9599	0.8969
median2	0.9887	0.8703	0.8904	0.9268	0.8200	0.8789	0.9569	0.9481	0.9365	0.8774
median5	0.9917	0.8475	0.8721	0.9136	0.8814	0.8705	0.9327	0.9265	0.9356	0.8679
median8	0.9863	0.6246	0.5960	0.7626	0.7812	0.6834	0.8449	0.8303	0.8776	0.7860

Table 4: MODEL_GAUS134_SNP010510 DSCs on the 16 held-out test datasets. The left-most column indicates which dataset was used for testing the model. Rows highlighted in green represent settings where the model achieves over 0.9 DSC for all classes.

Class	1	2	3	4	5	6	7	8	9	10
t2norm	0.9928	0.9462	0.9521	0.9645	0.9083	0.9424	0.9718	0.9634	0.9614	0.9211
gaus1	0.9927	0.9452	0.9500	0.9634	0.9064	0.9447	0.9724	0.9636	0.9619	0.9206
gaus2	0.9918	0.8987	0.9089	0.9264	0.8805	0.9137	0.9621	0.9568	0.9536	0.9083
gaus3	0.9910	0.8926	0.8968	0.9225	0.8641	0.9174	0.9615	0.9549	0.9507	0.9000
gaus4	0.9897	0.8577	0.8594	0.8914	0.8392	0.9028	0.9552	0.9488	0.9441	0.8829
gaus5	0.9856	0.7298	0.7312	0.7946	0.7591	0.8291	0.9277	0.9260	0.9174	0.8386
snp01	0.9928	0.9487	0.9542	0.9662	0.9092	0.9443	0.9726	0.9638	0.9619	0.9209
snp03	0.9928	0.9506	0.9556	0.9673	0.9100	0.9456	0.9730	0.9644	0.9620	0.9201
snp05	0.9928	0.9510	0.9557	0.9671	0.9099	0.9450	0.9732	0.9639	0.9622	0.9178
snp07	0.9927	0.9511	0.9554	0.9666	0.9092	0.9443	0.9721	0.9636	0.9627	0.9168
snp10	0.9926	0.9506	0.9542	0.9655	0.9078	0.9441	0.9719	0.9621	0.9611	0.9164
snp15	0.9923	0.9456	0.9463	0.9586	0.9025	0.9284	0.9680	0.9548	0.9549	0.9003
snp20	0.9907	0.9299	0.9195	0.9374	0.8833	0.8839	0.9486	0.9296	0.9440	0.8602
median2	0.9890	0.8701	0.8824	0.9208	0.8171	0.8841	0.9592	0.9457	0.9342	0.8788
median5	0.9927	0.8830	0.9102	0.9430	0.8918	0.8850	0.9610	0.9536	0.9504	0.9019
median8	0.9886	0.7279	0.7741	0.8445	0.7929	0.7446	0.9241	0.9262	0.9124	0.8439

enough segmentation for the Gaussian datasets with the highest σ value and none of these models generalised on the salt and pepper filtered images. A model trained on median filtered images (MODEL_MEDIAN5) showed only a little generalisation for Gaussian images but not for the salt and pepper images as was the case with the Gaussian trained models. The model only generalised a little on a heavier filtered median image.

Interestingly, a model trained on light salt and pepper noise (MODEL_SNP01) generalised rather well, even on data with heavier salt and pepper noise of up to snp07 as well as on the original DHCP images and lightly texturised of Gaussian and median images. Unlike the Gaussian image trained models, salt and pepper image trained models generalised well on all the lighter salt and pepper images and on some heavier noises. Noteworthy, when the dataset used to train the model had heavier noise in them, the performance of the model on median and normal DHCP appeared to be better (Table 3). Our findings therefore suggest that models trained on speckle textured images generalise well on other speckle generated images as well as on median smoothed images, which could mean that the model became more robust to textural bias, and hence used more information about the global structure of the images when carrying out segmentation. Models trained on smoother images, however, only generalised to images smoothed to similar degrees and not on the images smoothed using other technique.

Finally the model trained on different degrees of Gaussian and salt and pepper applied datasets (MODEL_GAUS134_SNP010510) showed the best performance across all datasets, where even the heaviest filtered images were only

missing some detail. Fig. 5 shows the predicted segmentations of the model on the heaviest transformed images of the three filters used in this investigation (MODEL_GAUS134_SNP010510). From the figure it is clear that the model achieved good segmentation on all of them, albeit missing some detail in median8 and gaus5.

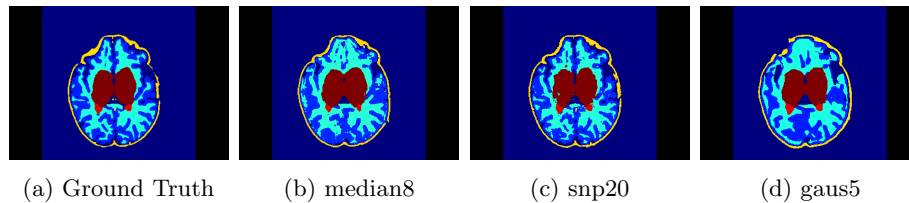


Fig. 5: Axial slices of the predicted segmentations of MODEL_GAUS134_SNP010510.

In terms of extending the investigation further, the next step would be to conduct a similar experiment on more permutations of smoothing, speckle generating, or even contrast changing filters to see if training models in these settings yield better segmentation results. Additionally, an investigation on whether this hypothesis works for actual domain shift of neuroimaging data, ideally using data generated across different domains is the natural next step. If this works, the research could be extended further to other medical images that currently require domain adaptation.

In conclusion, the findings of this investigation suggest a possibility for easing the domain shift problem in medical imaging, by introducing various levels of speckle patterns and smoothing to the images' textures prior to training.

4 Acknowledgments

The research leading to these results has received funding from the European Research Council under the European Union's Seventh Framework Programme (FP/2007-2013)/ERC Grant Agreement no. 319456. We are grateful to the families who generously supported this trial.

References

1. Yann LeCun, Yoshua Bengio and Geoffrey Hinton, F.: Deep Learning. *Nature* 521, 436–444 (2015)
2. Robert Geirhos, Patricia Rubisch, Claudio Michaelis, Matthias Bethge, Felix A. Wichmann and Wieland Brendel, F.: Imagenet-trained CNNs are biased towards texture; increasing shape bias improves accuracy and robustness. In *International Conference on Learning Representations* (2019) <https://openreview.net/forum?id=Bygh9j09KX>

3. Weiming Lin, Tong Tong, Qinquan Gao, Di Guo, Xiaofeng Du, Yonggui Yang, Gang Guo, Min Xiao, Min Du and Xiaobo Qu, F.: Convolutional Neural Networks-Based MRI Image Analysis for the Alzheimer’s Disease Prediction From Mild Cognitive Impairment, *Frontiers in Neuroscience* 12, 777 (2018)
4. R. Vinoth and Chunchu Venkatesh, F.: Segmentation and Detection of Tumor in MRI images Using CNN and SVM Classification. 2018 Conference on Emerging Devices and Smart Systems (ICEDSS), 21–25 (2018)
5. Li-Qiang Zhou, F.: Artificial Intelligence in Medical Imaging of the Liver. *World j Gastroenterol*, 672 – 682, (2019)
6. Konstantinos Kamnitsas, Christian Baumgartner, Christian Ledig, Virginia F.J. Newcombe, Joanna P. Simpson, Andrew D. Kane, David K. Menon, Aditya Nori, Antonio Criminisi, Daniel Rueckert, Ben Glocker, F.: Unsupervised Domain Adaptation in Brain Lesion Segmentation with Adversarial Networks. *Information Processing in Medical Imaging*, 597–609 (2017)
7. Xun Huang and Serge Belongie, F.: Arbitrary Style Transfer in Real-Time with Adaptive Instance Normalization. 2017 IEEE International Conference on Computer Vision (ICCV), 1510-1519 (2017)
8. Kaiming He, Xiangyu Zhang, Shaoqing Ren and Jian Sun, F.: Deep Residual Learning for Image Recognition. 2016 IEEE Conference on Computer Vision and Pattern Recognition (CVPR) (2016)
9. Adam Paszke, Sam Gross, Francisco Massa, Adam Lerer, James Bradbury, Gregory Chanan, Trevor Killeen, Zeming Lin, Natalia Gimelshein, Luca Antiga, Alban Desmaison, Andreas Kopf, Edward Yang, Zachary DeVito, Martin Raison, Alykhan Tejani, Sasank Chilamkurthy, Benoit Steiner, Lu Fang, Junjie Bai, and Soumith Chintala, F: PyTorch: An Imperative Style, High-Performance Deep Learning Library. *Advances in Neural Information Processing Systems* 32, 8024–8035 (2019)
10. Sebastien Marcel and Yann Rodriguez, F.: Torchvision the Machine-Vision Package of Torch. *Proceedings of the 18th ACM International Conference on Multimedia*, 1485–1488 (2010)
11. Matteo Bastiani, Jesper Andersson, Lucilio Cordero-Grande, Maria Murgasova, Jana Hutter, Anthony N. Price, Antonios Makropoulos, Sean P. Fitzgibbon, Emer Hughes, Daniel Rueckert, Suresh Victor, Mary Rutherford, A. David Edwards, Steve Smith, Jacques-Donald Tournier, Joseph V. Hajnal, Saad Jbabdi and Stamatios N. Sotiropoulos, F.: Automated Processing Pipeline for Neonatal Diffusion MRI in the Developing Human Connectome Project. *NeuroImage*, 750–763 (2018)
12. Christian S. Perone, Pedro Ballester, Rodrigo C. Barros and Julien Cohen-Adad, F.: Unsupervised Domain Adaptation for Medical Imaging Segmentation with Self-ensembling. *NeuroImage*, 1–11 (2019)
13. Max W. K. Law and Albert C. S. Chung, F.: Efficient Implementation for Spherical Flux Computation and Its Application to Vascular Segmentation. *IEEE Transactions on Image Processing* 18(3), 596–612 (2009)
14. Stefan van der Walt, Johannes L. Schönberger, Juan Nunez-Iglesias, François Boulogne, Joshua D. Warner, Neil Yager, Emmanuelle Gouillart and Tony Yu, F.: scikit-image: Image Processing in Python. *PeerJ* 2(6) (2014)
15. Konstantinos Kamnitsas, Christian Ledig, Virginia F.J. Newcombe, Joanna P. Simpson, Andrew D. Kane, David K. Menon, Daniel Rueckert and Ben Glocker, F.: Efficient multi-scale 3D CNN with fully connected CRF for accurate brain lesion segmentation. *Medical Image Analysis* 36(2), 61–78 (2017)
16. Yoshua Bengio, Aaron Courville and Pascal Vincent, F.: Representation Learning: A Review and New Perspectives. *IEEE Transactions on Pattern Analysis and Machine Intelligence* 35(8), 1798-1828 (2013)

17. Francesco Locatello, Stefan Bauer, Mario Lucic, Gunnar Rätsch, Sylvain Gelly, Bernhard Schölkopf and Olivier Bachem, F.: Challenging Common Assumptions in the Unsupervised Learning of Disentangled Representations. Proceedings of the 36th International Conference on Machine Learning (ICML 2019), (2018)